Supporting Information

Insights into the Structural Effects of Layered Cathode Materials for High Voltage Sodium-ion Batteries

Gui-Liang Xu,[1] Rachid Amine,[2, 3] Yue-Feng Xu,[4] Jianzhao Liu,[1,5] Jihyeon Gim, [1] Tianyuan Ma,[1, 6] Yang Ren,[7] Cheng-Jun Sun,[7] Yuzi Liu,[8] Xiaoyi Zhang,[7] Steve M. Heald,[7] Abderrahim Solhy, [9] Ismael Saadoune,[10] Wenjuan Liu Mattis,[11] Shi-Gang Sun,[4] Zonghai Chen[1,*] and Khalil Amine[1,*]

[1]*Chemical Sciences and Engineering Division, Argonne National Laboratory, Lemont, IL 60439, USA*

[2] *Chemical Engineering Department, University of Illinois at Chicago, Chicago, Illinois 60607, USA*

[3] *Materials Science Division, Argonne National Laboratory, 9700 S Cass Ave, Lemont, IL 60439, USA*

[4]*Collaborative Innovation Center of Chemistry for Energy Materials, State Key Laboratory Physical Chemistry of Solid Surfaces, Department of Chemistry, Xiamen University, Xiamen, 361005, China*

[5]*Department of Chemistry, Virginia Tech, 900 W Campus Drive, Blacksburg, VA 24061, USA*

[6] *Materials Science Program, University of Rochester, Rochester, NY 14627, USA*

[7]*X-ray Science Division, Argonne National Laboratory, Lemont, IL 60439, USA*

[8]*Center for Nanoscale Materials, Nanoscience Technology, Argonne National Laboratory, Lemont, IL 60439, USA*

[9]*Center for Advanced Materials, Mohammed VI Polytechnic University, Ben Guerir, Morocco*

[10] *Materials Science and Nano-engineering Department, Mohammed VI Polytechnic University, Ben Guerir, Morocco*

[11] *Microvast Inc., 12603 Southwest Freeway, Stafford, Texas 77477, USA*

To whom correspondence should be addressed:

Email: zonghai.chen@anl.gov (Z.C.) and amine@anl.gov (K.A.)

Table S1 Summary on the electrochemical performance of layered NaT_MO_2 (Tm=Ni, Co, Fe, Mn…) cathode materials for sodium-ion batteries

Materials	Rate, mA/g	1st coulombic efficiency	1st charge Capacity, mAh/g	Last Capacity, mAh/g	Voltage Range, V	Ref.
P2/O1/O3-$Na_xNi_{1/3}Co_{1/3}Mn_{1/3}O_2$	**15**	**95%**	**150.3**	**133/50th**	**2.0-4.4**	**This work**
P2/O1/O3-$Na_xNi_{1/3}Co_{1/3}Mn_{1/3}O_2$	**100**	**87.5%**	**143.6**	**100/100th**	**2.0-4.4**	**This work**
O3-$NaNi_{1/3}Co_{1/3}Mn_{1/3}O_2$	12	72%	156	112.3/1st	2.0-4.2	*Chem. Mater.* 2012, 24, 1846-1853.
O3-$NaNi_{0.5}Mn_{0.5}O_2$	8	74%	250	25/26th	2.0-4.5	*Inorg. Chem.*, 2012, 51, 6211-6220
Fe-doped O3 $NaFe_{0.2}Ni_{0.4}Mn_{0.4}O_2$	12	95%	136	125/30th	2.0-4.0	*ACS Appl. Mater. Interf.* 2015, 7, 8585-8591
O3 $NaTi_{0.5}Ni_{0.5}O_2$	20	87%	117	93/100th	2.0-4.0	*Chem. Commun.*, 2014, 50, 457-459
Li-doped O3 $NaLi_{0.07}Ni_{0.26}Mn_{0.4}Co_{0.26}O_2$	25	81.2%	181	128/50th	1.5-4.5	*Electrochem. Commun.* 2015, 60, 13-16.
P3-$Na_{0.5}Li_{0.5}Ni_{1/3}Co_{1/3}Mn_{1/3}O_2$	17	74.85%	201.3	89.8/30th	2.0-4.6	*J. Nanosci. Nanotechnol.* 16, 10698–10701, 2016
P2-$Na_{0.85}Li_{0.17}Ni_{0.21}Mn_{0.64}O_2$	15	80%	112	95/50th	2.0-4.2	*Adv. Energy Mater.* 2011, 1, 33-336
Zn-doped P2-$Na_{0.66}Ni_{0.26}Zn_{0.07}Mn_{0.67}O_2$	12	94%	150	118/30th	2.0-4.4	*J. Power Sources* 2015, 281, 18-26.
Mg doped P2-$Na_{0.67}Mn_{0.67}Ni_{0.28}Mg_{0.05}O_2$	17.3	94.6%	126.8	104.5/50th	2.5-4.35	*Angew. Chem. Int. Ed.* 2016, 55, 1-6
P2-$Na_{2/3}(Mn_{1/2}Fe_{1/4}Co_{1/4})O_2$	25.8	89.3%	168	130/30th	1.5-4.2	*Adv. Energy Mater.* 2015, 5, 1500944

P2-$Na_{0.67}Mn_{0.65}Co0.2Ni_{0.15}O_2$	20	>100%	N/A	123/50th	2.0-4.4	*J. Mater. Chem. A* 2013, 1(12): 3895.
P2-$Na_x(Fe_{1/2}Mn_{1/2})O_2$	N/A	>100%	121.3	101.4/80th	1.5-4.2	*Chem. Mater.* 2015, 27, 3150−3158
P2/O3-$Na_{0.8}Li_{0.2}Ni_{0.5}Mn_{0.5}O_2$	15	>100%	130	128/20th	2.0-4.05	*Adv. Energy Mater.* 2014, 4, 1400458
P2 $Na_{0.67}Ni_{0.33}Mn_{0.67}O_2$	17	>100%	130	40/100th	2.0-4.5	*Electrochim. Acta* 2013, 113, 200-204

Williamson-Hall analysis (http://pd.chem.ucl.ac.uk/pdnn/peaks/sizedet.htm)

This method is attributed to G.K.Williamson and his student, W.H.Hall (Acta Metall. 1, 22-31 (1953)). It relies on the principle that the approximate formulae for size broadening, β_L, and strain broadening, β_e, vary quite differently with respect to Bragg angle, θ:

$\beta_L = K\lambda/(L \cos\theta)$ Equation (1)

$\beta_e = C\varepsilon \tan\theta$ Equation (2)

One contribution varies as 1/cosθ and the other as tanθ. If both contributions are present then their combined effect should be determined by convolution. The simplification of Williamson and Hall is to assume the convolution is either a simple sum or sum of squares. Using the former of these then we get:

$\beta_{tot} = \beta_e + \beta_L = C\varepsilon \tan\theta + K\lambda/(L \cos\theta)$ Equation (3)

If we multiply Equation (3) by cosθ we get:

$\beta_{tot} \cos\theta = C\varepsilon \sin\theta + K\lambda/L$ *Equation (4)*

and comparing this to the standard equation for a straight line (m = slope; c = intercept)

$$y = mx + c$$

we see that by plotting $\beta_{tot}\cos\theta$ versus sinθ we obtain the strain component from the slope (Cε) and the size component from the intercept (Kλ/L).

The Williamson-Hall method has many assumptions: its absolute values should not be taken too seriously but it can be a useful method if used in the relative sense; for example a study of many powder patterns of the same chemical compound, but synthesized under different conditions, might reveal trends in the crystallite size/strain which in turn can be related to the properties of the product.

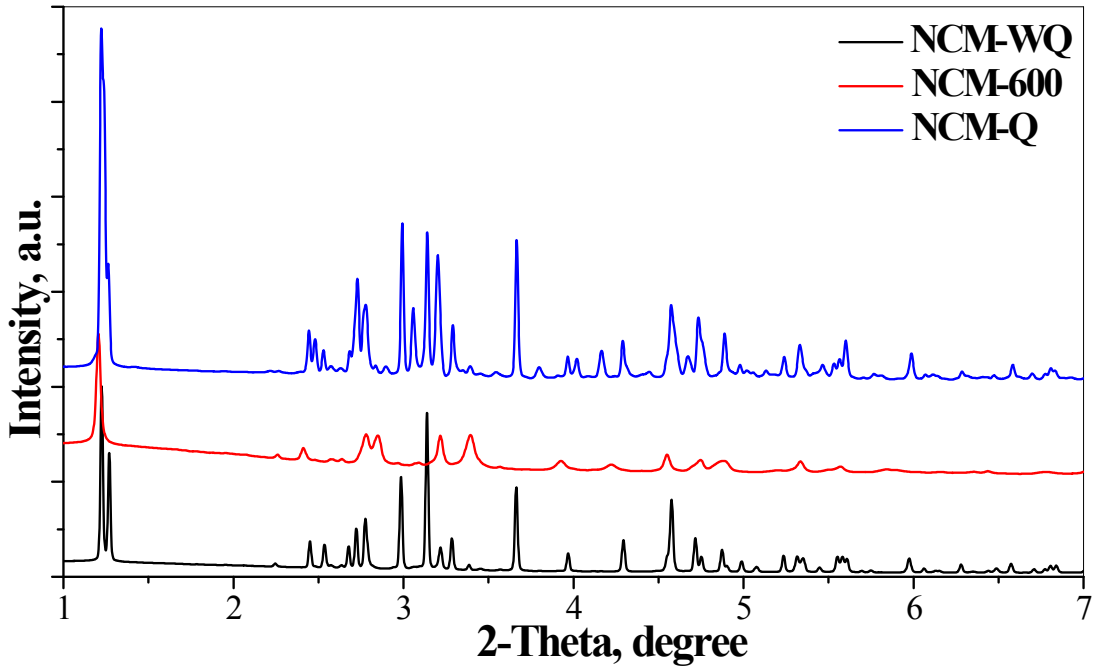

Figure S1 Synchrotron HEXRD patterns of NCM-Q, NCM-WQ and NCM-600.

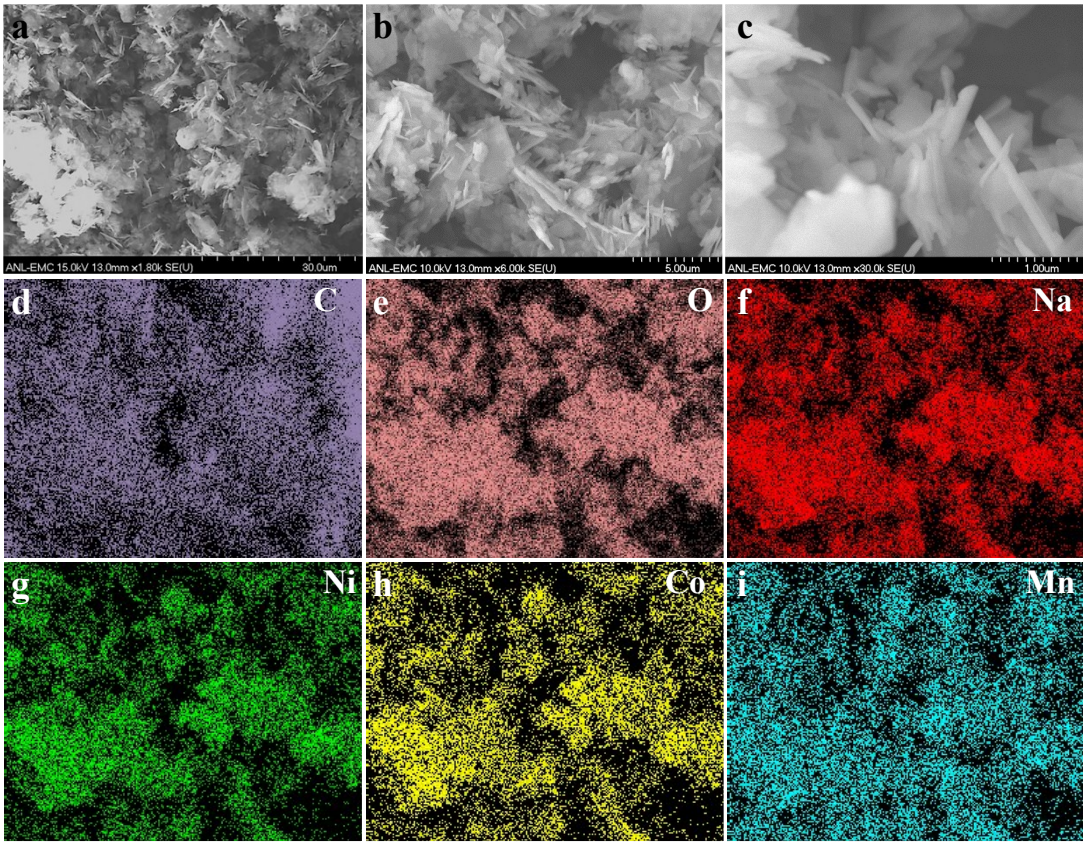

Figure S2 SEM images of the oxalate precursor (a-c) and the corresponding elemental mapping (d-i).

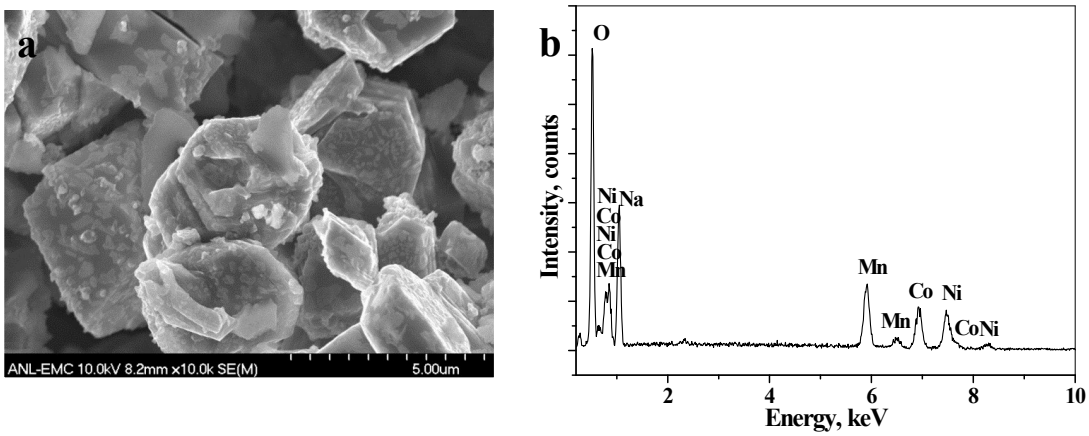

Figure S3 SEM image (a) and EDX analysis (b) of NCM-Q.

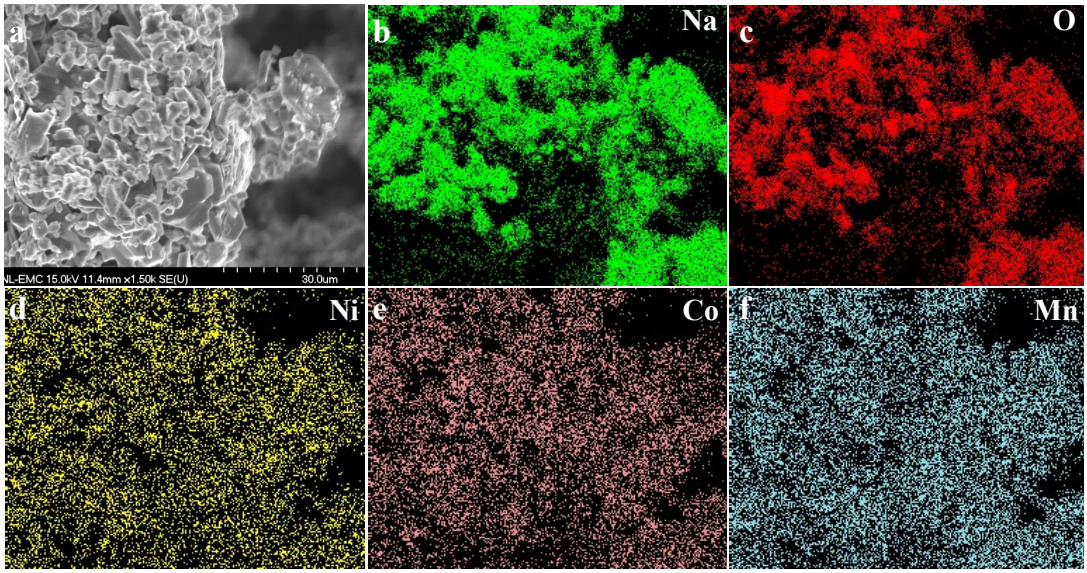

Figure S4 SEM images of NCM-Q and the corresponding elemental mapping.

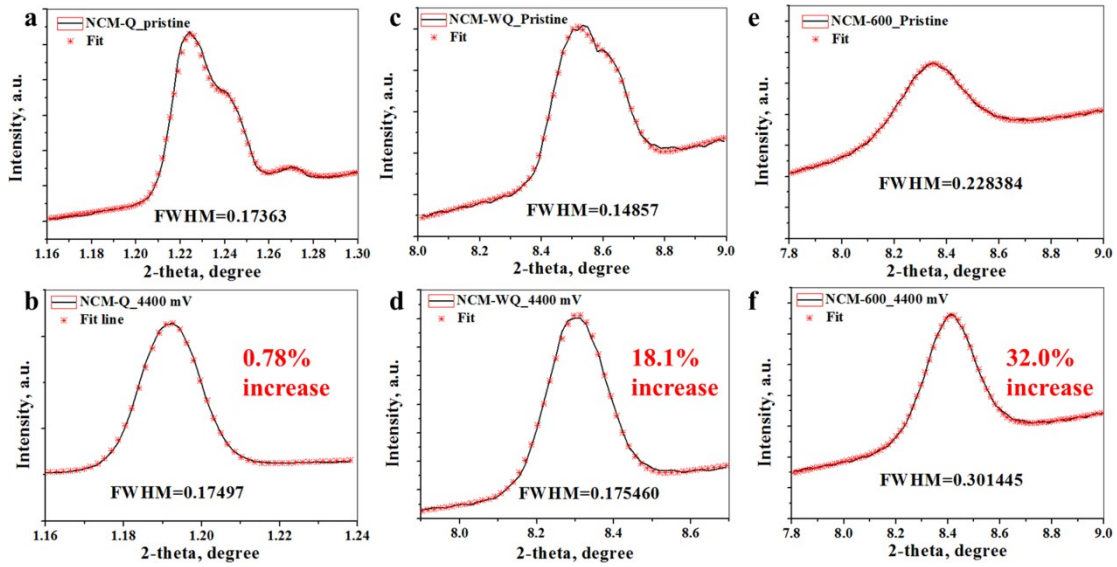

Figure S5 Fitting on the diffraction peak of NCM-Q (a, b), NCM-WQ (c, d) and NCM-600 (e, f) before and after charged to 4.4 V using CMPR software.

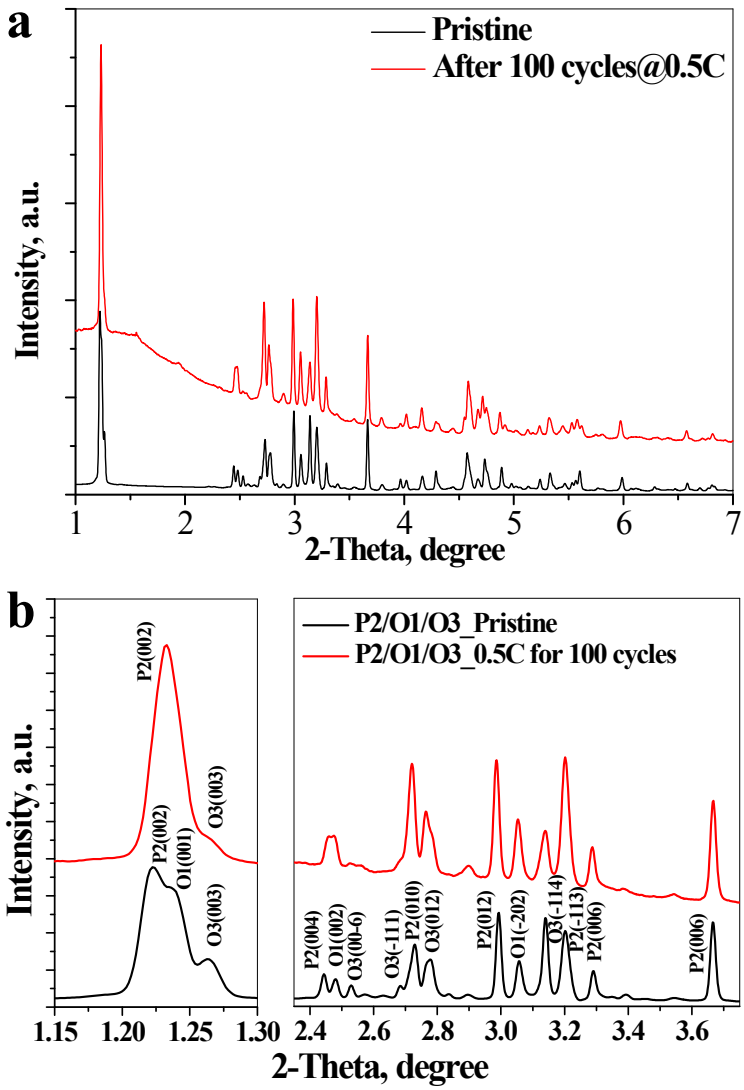

Figure S6 Full (a) and zoomed (b) synchrotron HEXRD patterns of pristine NCM-Q electrode and after cycled at 0.5 C for 100 cycles.

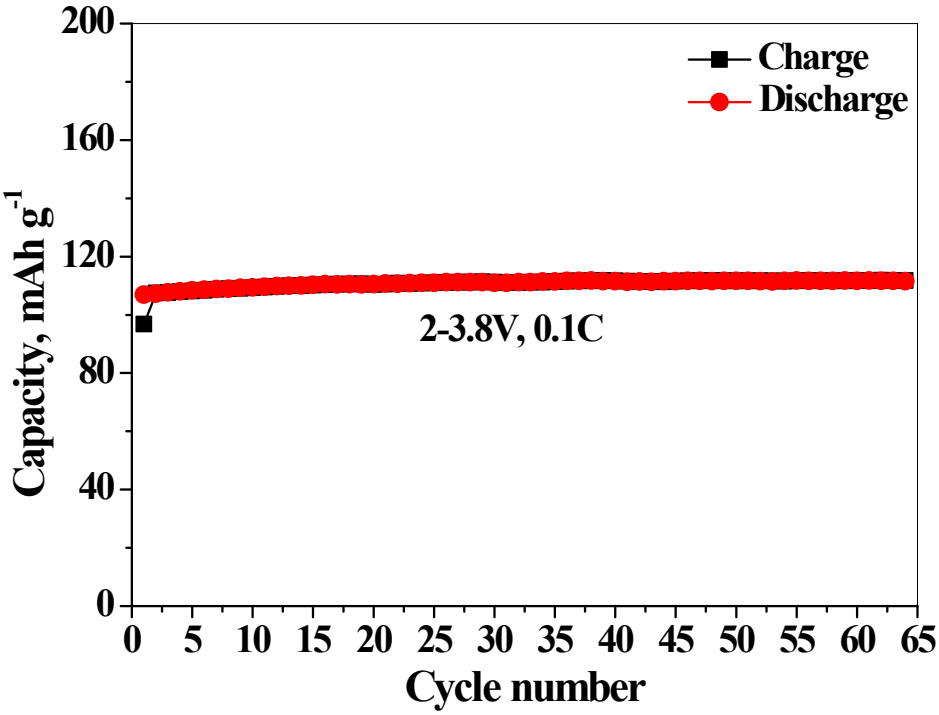

Figure S7 Cycle performance of NCM-Q electrode at 0.1 C within 2.0-3.8 V.

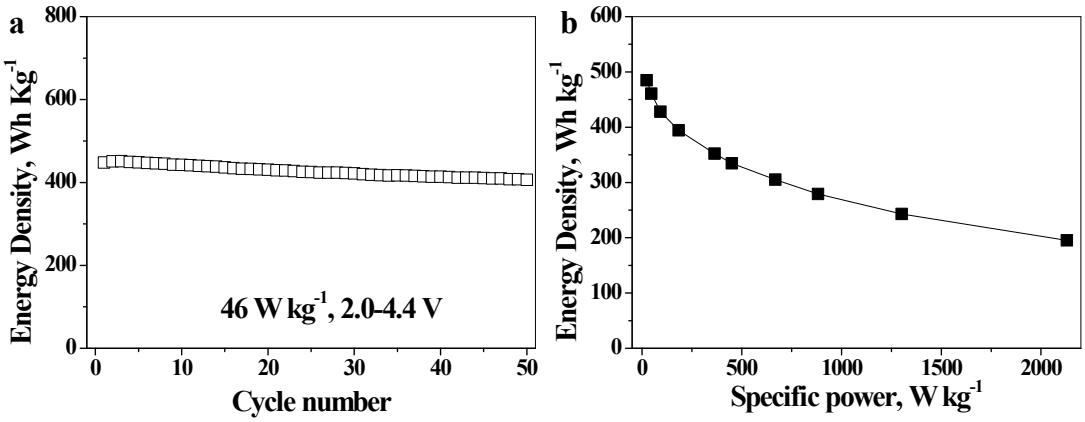

Figure S8 a) Energy density and b) power density of NCM-Q.

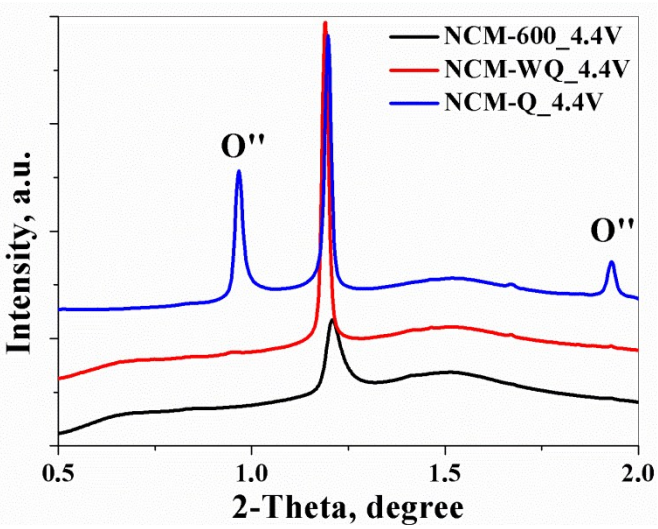

Figure S9 HEXRD patterns of deep-charged NCM-Q, NCM-WQ and NCM-600 (4.4V).

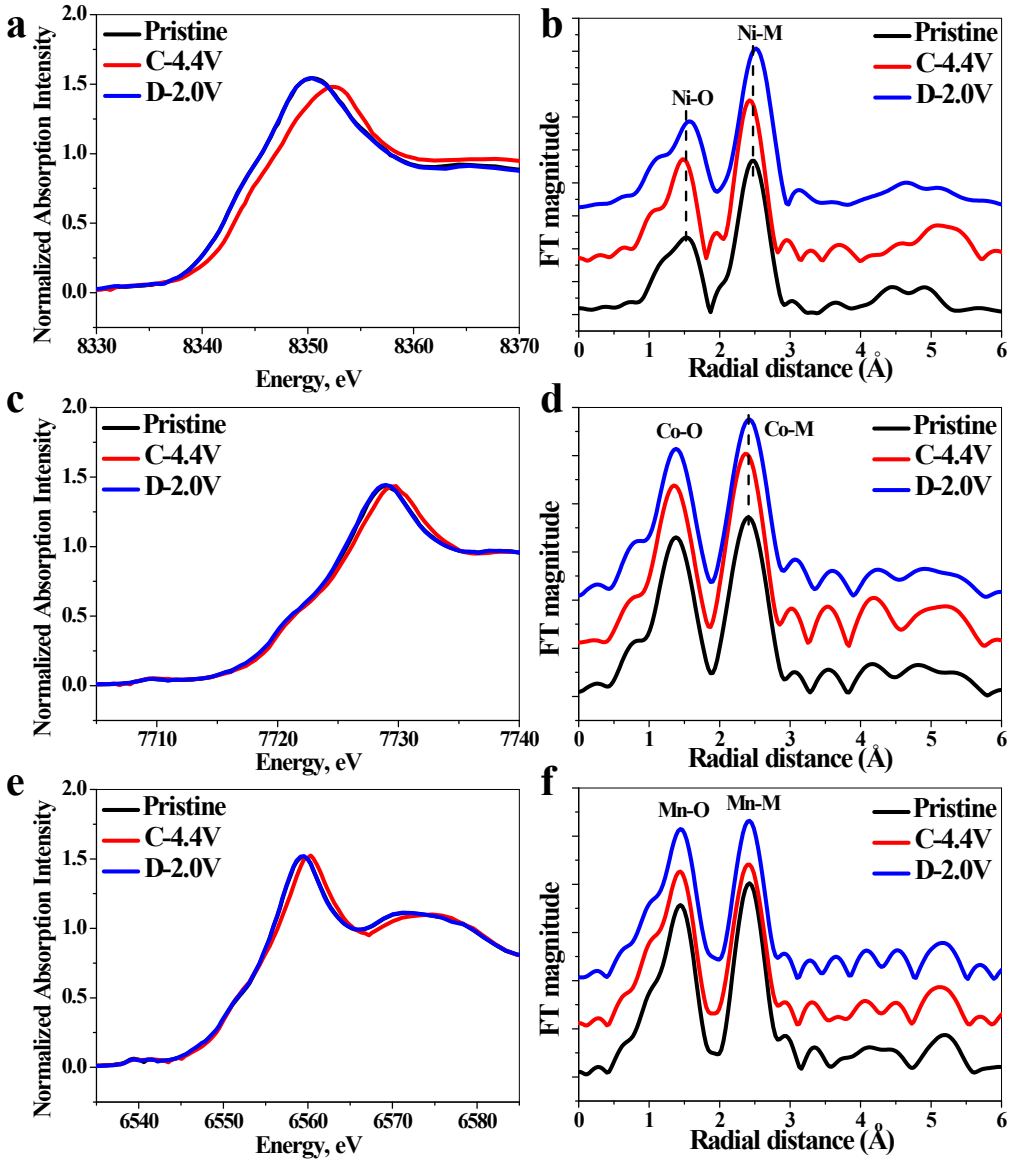

Figure S10 *Ex-situ* XANES and EXAFS spectra of the NCM-WQ electrode at different charge/discharge states: (a, d) Ni K-edge; (b, e) Co K-edge and (c, f) Mn K-edge. C for charge and D for discharge.

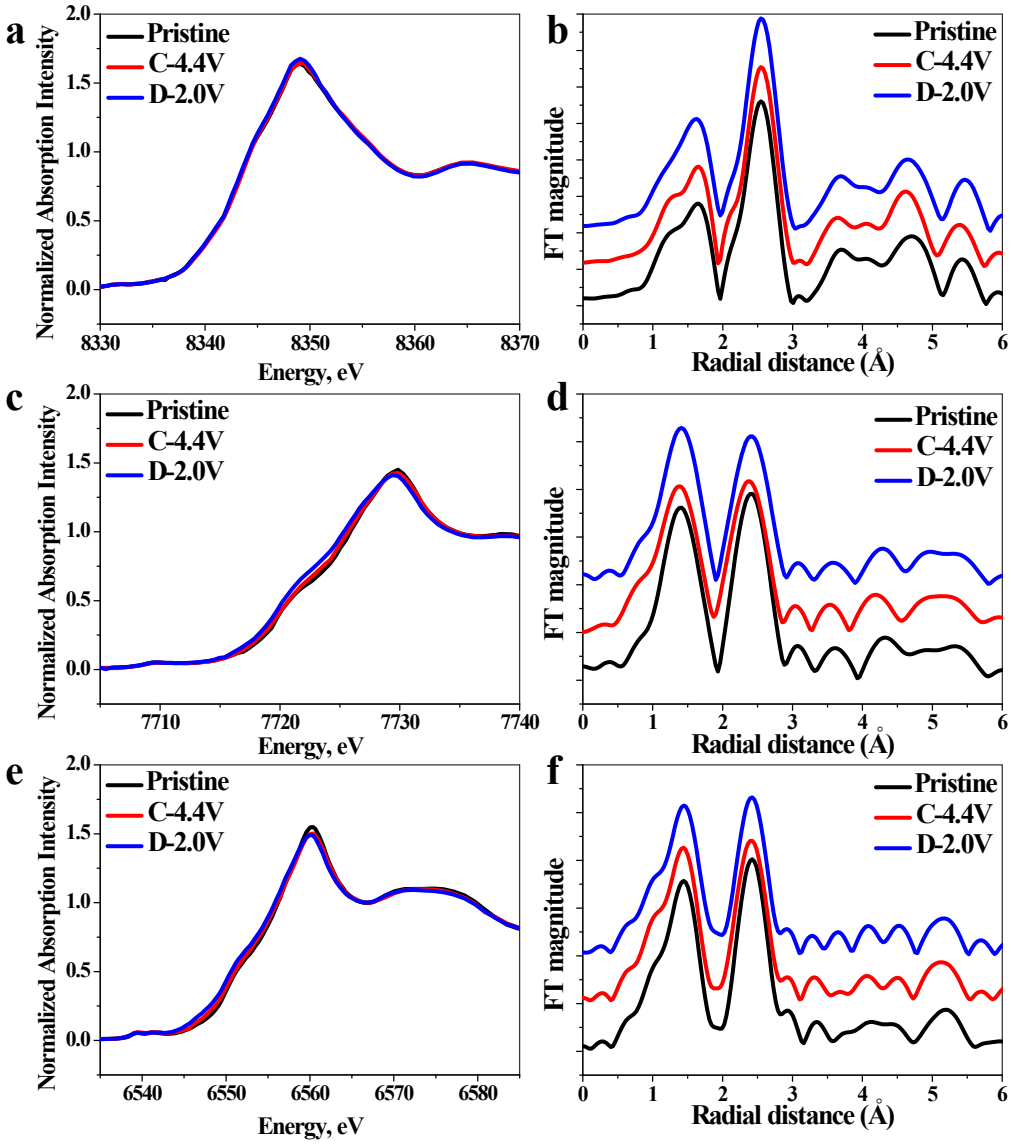

Figure S11 *Ex-situ* XANES and EXAFS spectra of the NCM-600 electrode at different charge/discharge states: (a, d) Ni K-edge; (b, e) Co K-edge and (c, f) Mn K-edge. C for charge and D for discharge.

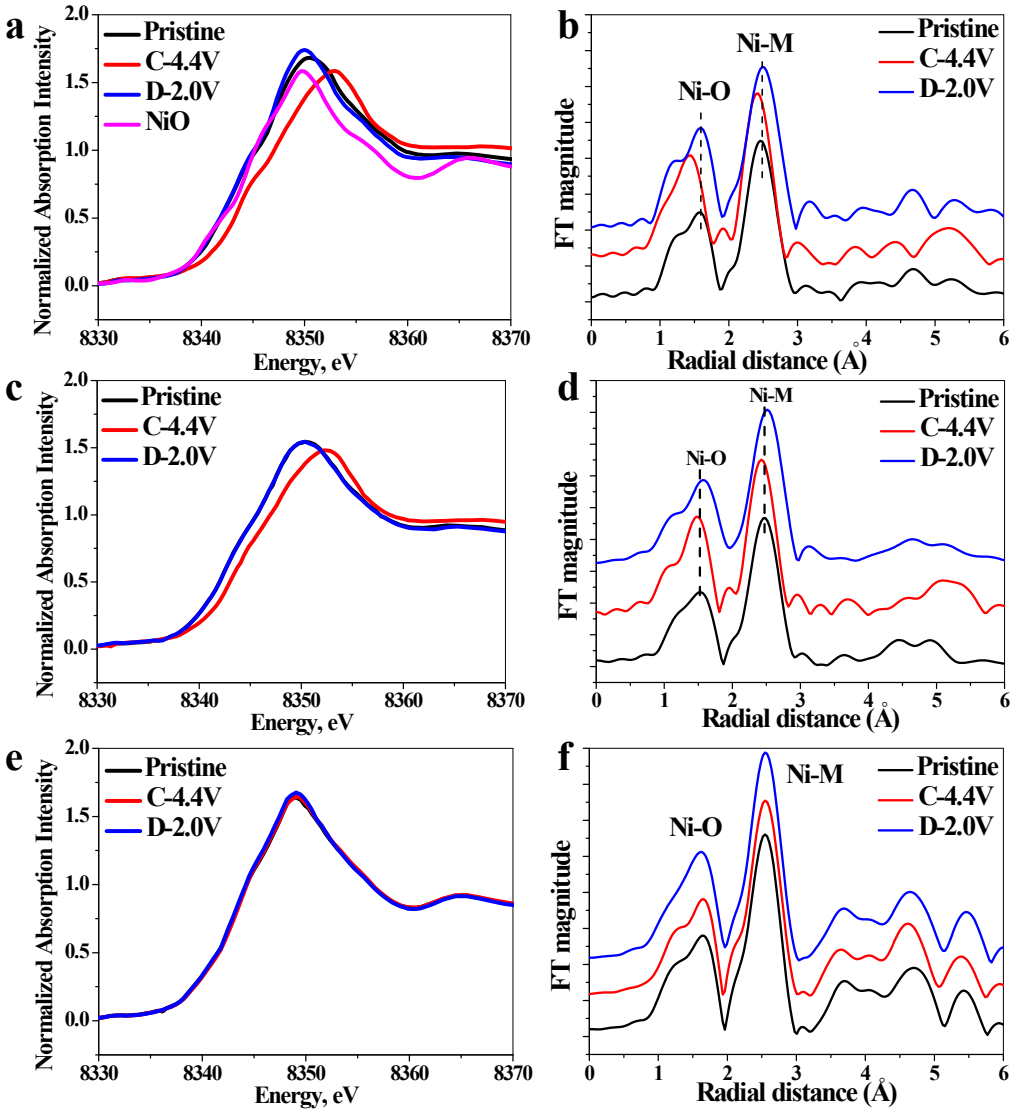

Figure S12 *Ex-situ* Ni K-edge XANES and EXAFS for NCM-Q (a, b), NCM-WQ (c, d) and NCM-600 (e, f) at different charge/discharge states. C for charge and D for discharge.

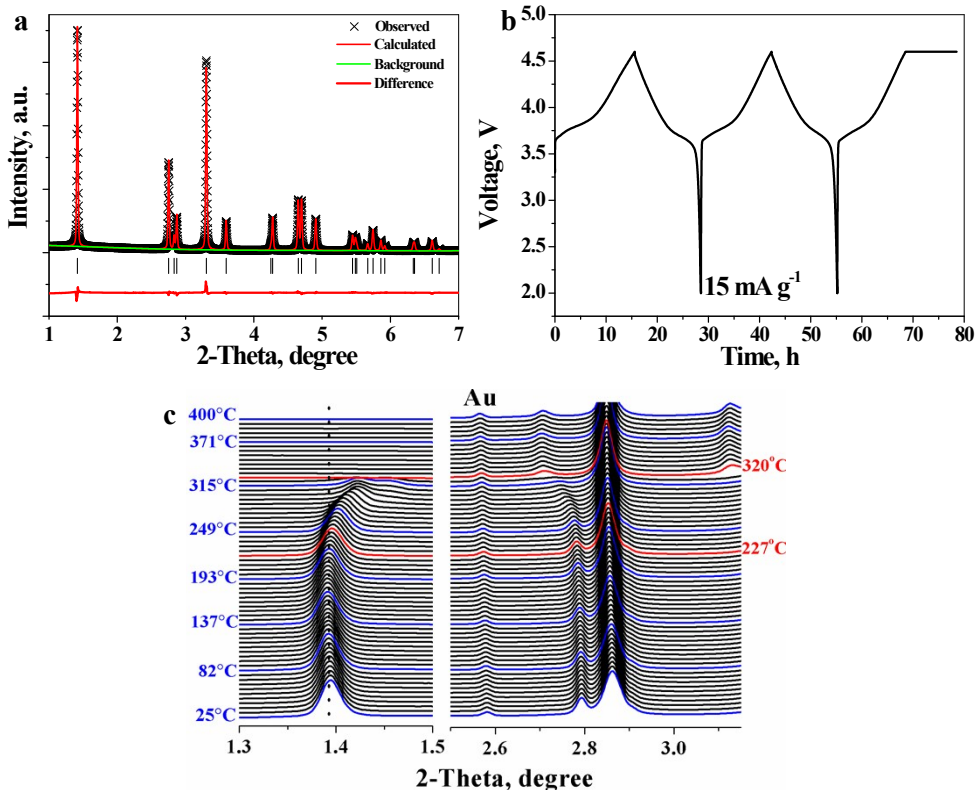

Figure S13 a) Rietveld refinement of HEXRD pattern and b) charge/discharge curves of LiNCM-333, c) *in-situ* HEXRD pattern of de-lithiated LiNCM-333 with the presence of 2 μL electrolytes (1M $LiPF_6$/EC+DMC).